Journal of Sound and Vibration (1997) **207**(4), 521–535

THE RESPONSE OF TWO-DIMENSIONAL PERIODIC STRUCTURES TO HARMONIC POINT LOADING: A THEORETICAL AND EXPERIMENTAL STUDY OF A BEAM GRILLAGE

R. S. Langley and N. S. Bardell

Department of Aeronautics and Astronautics, University of Southampton, Southampton SO17 1BJ, England

and

H. M. Ruivo

Directotia de Engenharia Naval, Praça Mauá, 65—Centro, Rio de Janeiro, Brazil

(*Received* 19 *March* 1997, *and in final form* 13 *June* 1997)

This work is concerned with the response of a beam grillage system to a harmonic point load. This system serves as a particular example of a two-dimensional periodic structure, and the aim of the work is to validate a number of recent results regarding the general nature of the response of such structures to a localized excitation source. The grillage is analyzed by using the hierarchical finite element method to model a single period and then employing periodic structure theory to yield the "phase constant surfaces" which are needed for the forced response analysis. The theoretical work is complemented by an experimental study of a grillage system; a relatively high level of damping treatment is employed to produce a non-reverberant system that behaves in a similar manner to an infinitely extended system. Both the theoretical and experimental results show that the response can exhibit highly directional "beaming", the spatial pattern of which is strongly dependent on the excitation frequency, and this finding is fully consistent with the findings of the aforementioned general study.

1. INTRODUCTION

Any structure which is constructed by repeating a basic structural unit to form a regular pattern is known as a periodic structure. Such structures occur widely in engineering, with a prime example consisting of an orthogonally stiffened plate or shell: here the basic structural unit can be considered to be an edge stiffened panel which is repeated in two directions to form the complete system. In this case the system is said to be a *two-dimensional* periodic structure, and much previous research effort has been directed at the dynamic behaviour of structures of this type. The motivation for this work has arisen from the fact that many engineering structures are subjected to significant dynamic loading, and this can lead to excessive noise and vibration levels and/or fatigue damage unless dynamic response is considered at the design stage.

The majority of previous work on two-dimensional periodic structures has been concerned with the propagation of free plane wave motion through the system and/or the response of the system to plane pressure wave excitation (as summarized in two recent review papers [1, 2]). In the case of free plane wave motion, the system can be analyzed

0022–460X/97/440521 + 15 $25.00/0/sv971154

by applying Bloch's theorem [3] to a mathematical model of a single period; examples of this approach are given in reference [4] for an orthogonally stiffened plate and in reference [5] for an orthogonally stiffened shell—in each case the hierarchial finite element method was used to model the single period. The response of the system to pressure wave excitation can also be analyzed by considering a single period, and this approach is described in references [6] and [7] for the case of a stiffened plate. The response of a two-dimensional periodic structure to localized forcing, such as a point load, is more problematical, since the system response will not be homogeneous (i.e., of the same form in each period) and thus it is not obvious that the response can be predicted by considering a single period alone. This issue has recently been addressed in reference [8] for the case of harmonic point loading and in reference [9] for the case of impulsive point loading. In each case it was shown that the response can in fact be expressed in terms of the plane wave components which are yielded by a free vibration analysis of a single periodic unit, and the developed theory was applied to a simple two-dimensional periodic mass–spring system. For harmonic excitation it was shown that the system response can display very distinctive "beaming" behaviour at certain frequencies, with significant motion being restricted to narrow directional bands radiating from the point load. While this type of behaviour is certainly predicted theoretically for the simple mass–spring system considered in reference [8], two points remain to be proven: (i) whether beaming will occur for more complex and more realistic two-dimensional periodic structures; and (ii) whether beaming can clearly be observed in an experimental structure. With regard to point (ii) it can be noted that beaming has very recently been observed by applying acoustic holography measurement techniques to a point loaded ribbed shell [10]. The ribbed shell is basically a one-dimensional periodic structure, in the sense that the ribs lead to structural periodicity in the axial direction only, although the surface of the shell does of course form a two-dimensional region. In the present work, points (i) and (ii) are investigated for a truly two-dimensional periodic system via a theoretical and experimental study of a beam grillage system. This serves to illustrate and validate the theory presented in reference [8] for a realistic engineering structure which has been the subject of previous studies regarding free wave motion [11].

A beam grillage is perhaps the simplest form of continuum two-dimensional periodic structure which can be tested experimentally, and in the present work a beam grillage constructed from strips of aluminium with bolted joints is considered. The response of the system to a harmonic point load is computed by employing the analysis of reference [8] in conjunction with an hierarchical finite element model of a single period. The predicted response is then compared with experimental results and an excellent qualitative and good quantitative level of agreement is demonstrated. In particular, the beaming behaviour predicted in reference [8] is observed clearly in both the theoretical and experimental results.

2. ANALYSIS OF FREE WAVE MOTION IN A PERIODIC BEAM GRILLAGE

2.1. HIERARCHICAL FINITE ELEMENT ANALYSIS OF A SINGLE PERIOD

The present analysis is concerned with the beam grillage system which is shown schematically in Figure 1. The grillage is a two-dimensional periodic structure in the sense that the complete system can be constructed by repeating a single "period" (highlighted in Figure 1) in both the x_1 and x_2 directions. As a preliminary to modelling free wave motion through the system, it is necessary to develop a mathematical model of the single period, and in this regard the present analysis is restricted to the consideration of torsion

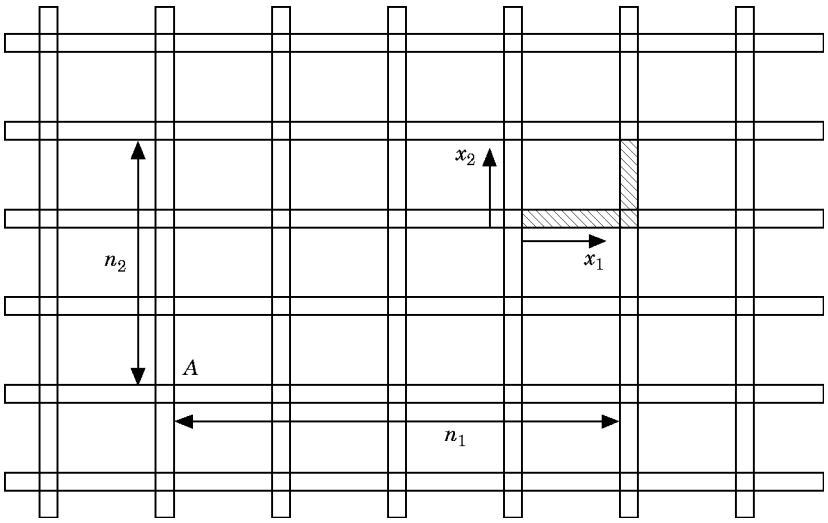

Figure 1. A schematic of a periodic beam grillage system with a single period highlighted. The point A represents the reference node.

and out-of-plane bending of the beam components: it is assumed that in-plane bending and axial vibrations occur at frequencies beyond the current range of interest, and this is certainly true for the experimental structure described in section 4.

The period highlighted in Figure 1 is modelled in what follows by using two hierarchical finite elements, so that the system has three nodes, as indicated in Figure 2. Taking the first element as an example, the out-of-plane displacement w and torsional rotation θ are expressed in the form

$$w(x, t) = \sum_{r=1}^{N} a_r(t) f_r(x), \qquad \theta(x, t) = \sum_{r=1}^{M} b_r(t) g_r(x), \tag{1, 2}$$

where x is measured along the beam axis. The out-of-plane degrees of freedom a_r consist of the four nodal degrees of freedom $(w_1\ \psi_1\ w_2\ \psi_2)$ shown in Figure 2, together with a set of internal generalized degrees of freedom which make no contribution to the displacement

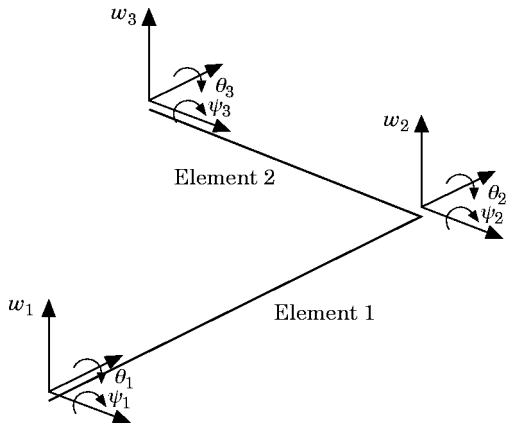

Figure 2. A two-element hierarchical finite element model of a single period. Note that for element 2, θ_2 and θ_3 are bending degrees of freedom, while ψ_2 and ψ_3 are torsional degrees of freedom.

and slope at either end of the element. The shape functions $f_r(x)$ associated with the nodal degrees of freedom are the standard cubic polynomials which are employed in a conventional beam finite element [12], while those associated with the generalized degrees of freedom are based on Legendre polynomials, as detailed in reference [13]. The first two torsional degrees of freedom b_r which appear in equation (2) represent the nodal rotations $(\theta_1\ \theta_2)$ shown in Figure 2, while the remaining degrees of freedom represent internal rotations. In this case $g_1(x)$ and $g_2(x)$ are linear shape functions, while the subsequent terms are Legendre polynomials with $g_r(0) = g_r(L) = 0$, where L is the length of the element [14]. Full mathematical details of the hierarchical finite element method are available in references [13] and [14], and the shape functions $f_r(x)$ and $g_r(x)$ are plotted in reference [14].

Given the assumed displacements in the form of equations (1) and (2), the kinetic energy of the beam element can be written as [15]

$$T = (1/2)\sum_{r=1}^{N}\sum_{s=1}^{N}\dot{a}_r\,\dot{a}_s\int_0^L mf_r(x)f_s(x)\,\mathrm{d}x + (1/2)\sum_{r=1}^{M}\sum_{s=1}^{M}\dot{b}_r\,\dot{b}_s\int_0^L I_p\,g_r(x)g_s(x)\,\mathrm{d}x, \quad (3)$$

where m and I_p are, respectively, the mass and polar moment of inertia per unit length. Similarly, the strain energy of the element can be written as [15]

$$U = (1/2)\sum_{r=1}^{N}\sum_{s=1}^{N}a_r\,a_s\int_0^L EIf_r''(x)f_s''(x)\,\mathrm{d}x + (1/2)\sum_{r=1}^{M}\sum_{s=1}^{M}b_r\,b_s\int_0^L GJg_r'(x)\,g_s'(x)\,\mathrm{d}x, \quad (4)$$

where EI and GJ are the flexural and torsional rigidities of the beam. The integrals that appear in equations (3) and (4) can be evaluated by employing symbolic computing, as detailed in reference [14]. The equations of motion of the element then follow from Lagrange's equation, which states [15] that

$$\frac{\mathrm{d}}{\mathrm{d}t}\left(\frac{\partial T}{\partial \dot{u}_r}\right) - \frac{\partial T}{\partial u_r} + \frac{\partial U}{\partial u_r} = 0, \quad (5)$$

where u_r represents either a_r or b_r. Having derived the equations of motion of each of the two elements in this way, the equations of motion of the complete period can be assembled by enforcing compatibility at the coupling point (node 2); the resulting equations can then be written conveniently in the following partitioned matrix form

$$\begin{bmatrix} \mathbf{M}_{11} & \mathbf{M}_{12} & \mathbf{M}_{13} & \mathbf{M}_{1I} \\ \mathbf{M}_{12}^{\mathrm{T}} & \mathbf{M}_{22} & \mathbf{M}_{23} & \mathbf{M}_{2I} \\ \mathbf{M}_{13}^{\mathrm{T}} & \mathbf{M}_{23}^{\mathrm{T}} & \mathbf{M}_{33} & \mathbf{M}_{3I} \\ \mathbf{M}_{1I}^{\mathrm{T}} & \mathbf{M}_{2I}^{\mathrm{T}} & \mathbf{M}_{3I}^{\mathrm{T}} & \mathbf{M}_{II} \end{bmatrix} \begin{bmatrix} \ddot{\mathbf{u}}_1 \\ \ddot{\mathbf{u}}_2 \\ \ddot{\mathbf{u}}_3 \\ \ddot{\mathbf{u}}_I \end{bmatrix} + \begin{bmatrix} \mathbf{K}_{11} & \mathbf{K}_{12} & \mathbf{K}_{13} & \mathbf{K}_{1I} \\ \mathbf{K}_{12}^{\mathrm{T}} & \mathbf{K}_{22} & \mathbf{K}_{23} & \mathbf{K}_{2I} \\ \mathbf{K}_{13}^{\mathrm{T}} & \mathbf{K}_{23}^{\mathrm{T}} & \mathbf{K}_{33} & \mathbf{K}_{3I} \\ \mathbf{K}_{1I}^{\mathrm{T}} & \mathbf{K}_{2I}^{\mathrm{T}} & \mathbf{K}_{3I}^{\mathrm{T}} & \mathbf{K}_{II} \end{bmatrix} \begin{bmatrix} \mathbf{u}_1 \\ \mathbf{u}_2 \\ \mathbf{u}_3 \\ \mathbf{u}_I \end{bmatrix} = \begin{bmatrix} \mathbf{0} \\ \mathbf{0} \\ \mathbf{0} \\ \mathbf{0} \end{bmatrix}. \quad (6)$$

Here $\mathbf{u}_i = (w_i\ \psi_i\ \theta_i)$ represents the deflection of node i (for $i = 1$, 2 and 3), and $\mathbf{u}_I$ represents the complete set of internal degrees of freedom (both out-of-plane and torsion) for the two element assembly. The nodal degrees of freedom are shown in Figure 2, while the internal degrees of freedom represent the amplitudes of the hierarchical shape functions; as mentioned previously, these shape functions do not contribute to the displacements or rotations at the nodal points.

In the experimental structure considered in section 4, the beams are bolted together at the connection point (node 2) and the bolt contributes a significant local mass; this is allowed for in the present model by adding the bolt mass to the first diagonal entry of $\mathbf{M}_{22}$. As described in the following section, the equations of motion of the single period, equation (6), can be used to study the propagation of wave motion through the complete system.

2.2. ANALYSIS OF FREE WAVE MOTION

Free harmonic wave motion through a periodic system can be analyzed by employing Bloch's theorem, which states that the change in the complex wave amplitude across a period does not depend upon the location of the period within the system. In the present notation, the theorem takes the form $\mathbf{u}_2 = \exp(\lambda_1)\mathbf{u}_1$ and $\mathbf{u}_3 = \exp(\lambda_2)\mathbf{u}_2$, where the constants λ_1 and λ_2 are functions of the frequency ω of the wave motion but do not vary from period to period. If the wave motion propagates without attenuation in either the x_1 or the x_2 direction, then λ_1 and λ_2 will take the form $\lambda_1 = \mathrm{i}\varepsilon_1$ and $\lambda_2 = \mathrm{i}\varepsilon_2$, where ε_1 and ε_2 (with $-\pi < \varepsilon_i \leqslant \pi$ for uniqueness) are known as the phase constants of the motion. In this case Bloch's theorem for a single period can be expressed conveniently in the matrix form

$$\begin{bmatrix} \mathbf{u}_1 \\ \mathbf{u}_2 \\ \mathbf{u}_3 \\ \mathbf{u}_I \end{bmatrix} = \begin{bmatrix} \mathbf{I} & \mathbf{0} \\ \mathbf{I}e^{\mathrm{i}\varepsilon_1} & \mathbf{0} \\ \mathbf{I}e^{\mathrm{i}\varepsilon_1 + \mathrm{i}\varepsilon_2} & \mathbf{0} \\ \mathbf{0} & \mathbf{I} \end{bmatrix} \begin{pmatrix} \mathbf{u}_1 \\ \mathbf{u}_I \end{pmatrix} = \mathbf{R}\mathbf{u}, \tag{7}$$

where $\mathbf{R}$ and $\mathbf{u}$ are defined accordingly. This result can be combined with equation (6) to yield

$$\mathbf{R}^{*\mathrm{T}}\ (-\omega^2\mathbf{M} + \mathbf{K})\mathbf{R}\mathbf{u} = \mathbf{0}, \tag{8}$$

where $\mathbf{M}$ and $\mathbf{K}$ represent the matrices which appear in equation (6), and it has been noted that the motion is time harmonic with frequency ω. The use of the term $\mathbf{R}^{*\mathrm{T}}$ on the left of equation (8) ensures that the relevant force equilibrium conditions are satisfied by the wave motion [16]. Equation (8) can be re-expressed in the form

$$\{-\omega^2\mathbf{A}(\varepsilon_1, \varepsilon_2) + \mathbf{B}(\varepsilon_1, \varepsilon_2)\}\mathbf{u} = \mathbf{0}, \tag{9}$$

where the matrices $\mathbf{A}$ and $\mathbf{B}$ are derived from $\mathbf{M}$ and $\mathbf{K}$ via the transformation matrix $\mathbf{R}$. For specified ε_1 and ε_2, equation (9) represents an eigenproblem that can be solved to yield the eigenfrequencies ω and the associated eigenvectors $\mathbf{u}$; it can readily be verified that $\mathbf{A}$ and $\mathbf{B}$ are Hermitian matrices, which means that the eigenfrequencies are real. Physically, any triad $(\varepsilon_1, \varepsilon_2, \omega)$ resulting from equation (9) corresponds to a propagating plane wave, and a three-dimensional plot of the frequency ω against the ε_1–ε_2 plane will yield a so-called "phase constant surface" $\omega = \Omega(\varepsilon_1, \varepsilon_2)$ [1, 2]—clearly, multiple surfaces will arise in a plot of this type, since each point on the $\varepsilon_1 - \varepsilon_2$ plane is associated with multiple frequencies via equation (9).

It is convenient to describe the location of any point on the beam grillage via a combined global/local reference system of the form $(\mathbf{n}, \mathbf{x})$, where $\mathbf{n} = (n_1\, n_2)$ identifies the period containing the point and $\mathbf{x} = (x_1\, x_2)$ identifies the point location within the period, as shown in Figure 1. With this notation the out-of-plane wave motion $w(\mathbf{n}, \mathbf{x}, \varepsilon_1, \varepsilon_2)$ associated with a solution $\omega = \Omega(\varepsilon_1, \varepsilon_2)$ to equation (9) will have the form [3]

$$w(\mathbf{n}, \mathbf{x}, \varepsilon_1, \varepsilon_2) = \alpha(\mathbf{x}, \varepsilon_1, \varepsilon_2) \exp(\mathrm{i}\varepsilon_1 n_1 + \mathrm{i}\varepsilon_2 n_2 + \mathrm{i}\omega t), \tag{10}$$

where $\alpha(\mathbf{x}, \varepsilon_1, \varepsilon_2)$ is a complex amplitude function; this function can be constructed from the eigenvector $\mathbf{u}$ yielded by equation (9) in conjunction with the shape functions f_r and g_r which appear in equations (1) and (2). As discussed in the following section, the phase constant surfaces and the associated wave amplitude functions α can be used to compute the response of the system to harmonic point loading.

3. RESPONSE OF A BEAM GRILLAGE TO HARMONIC POINT LOADING

The response of a general two-dimensional periodic structure to harmonic point loading has been considered in reference [8]. In the present section, a slightly modified version of the analysis contained in reference [8] is applied to the beam grillage system shown in Figure 1.

The out-of-plane response $w(\mathbf{n}, \mathbf{x})$ of the grillage produced by a harmonic point load of frequency ω, location $(\mathbf{n}_0, \mathbf{x}_0)$, and complex amplitude F, can be expressed in the form of a modal expansion so that [15]

$$w(\mathbf{n}, \mathbf{x}) = \sum_p \sum_q \frac{F\phi_{pq}(\mathbf{n}_0, \mathbf{x}_0)\phi_{pq}(\mathbf{n}, \mathbf{x})}{(1 + \mathrm{i}\eta)\omega_{pq}^2 - \omega^2}, \tag{11}$$

where $\phi_{pq}(\mathbf{n}, \mathbf{x})$ are the modes of vibration of the system, ω_{pq} are the natural frequencies and η is the loss factor. The modes of vibration that appear in equation (11) are scaled to unit generalized mass so that

$$\sum_{n_1=1}^{N_1} \sum_{n_2=1}^{N_2} \int_A \rho(\mathbf{x})\phi_{pq}^2(\mathbf{n}, \mathbf{x})\, \mathrm{d}\mathbf{x} = 1, \tag{12}$$

where A represents the area of a period, $\rho(\mathbf{x})$ is the density (mass per unit area), and N_1 and N_2 are, respectively, the total number of periods in the x_1 and x_2 directions.

The modes of vibration $\phi_{pq}(\mathbf{n}, \mathbf{x})$ are strongly dependent on the boundary conditions which are applied to the system, and the forced response yielded by equation (11) will normally share this dependency. If, however, the system is highly damped, so that the disturbance produced by the point load decays significantly before reaching the system boundaries, then the response will be approximately independent of the boundary conditions, and any mathematically expedient set of boudary conditions can be employed to yield the mode shapes and natural frequencies which appear in equation (11). In this case it is convenient to employ the Born–Von Kármán boundary conditions [8], as the modes of vibration can then be expressed very simply in terms of propagating plane wave components; since the modes form a complete set of admissible functions, there is no need to consider evanescent forms of wave motion through the grillage system. The Born–Von Kármán boundary conditions, which were originally developed for solid-state physics applications [17], state that the left-hand edge of the system is contiguous with the right-hand edge, and similarly the top edge is contiguous with the bottom edge, so that the system is topologically equivalent to a torus. These conditions are satisfied by a plane wave in the form of equation (11) provided that $\varepsilon_1 = 2\pi p/N_1 \triangleq \varepsilon_{1p}$ and $\varepsilon_2 = 2\pi q/N_2 \triangleq \varepsilon_{2q}$ for integer values of p and q; the modes of vibration can be constructed by adding or substracting two waves which propagate in opposite directions, so that one wave has the phase constants $(\varepsilon_{1p}, \varepsilon_{2q})$ while the other has the constants $(-\varepsilon_{1p}, -\varepsilon_{2q})$. It follows from equations (7)–(10) that both of these waves propagate at the same frequency

$\omega_{pq} = \Omega(\varepsilon_{1p}, \varepsilon_{2q})$ and further that $\alpha(\mathbf{x}, -\varepsilon_{1p}, -\varepsilon_{2q}) = \alpha^*(\mathbf{x}, \varepsilon_{1p}, \varepsilon_{2q})$, so that the sum and difference of the waves leads to mode shapes of the form

$$\begin{Bmatrix} \phi_{1pq}(\mathbf{n}, \mathbf{x}) \\ \phi_{2pq}(\mathbf{n}, \mathbf{x}) \end{Bmatrix} = \begin{Bmatrix} \mathrm{Re} \\ \mathrm{Im} \end{Bmatrix} 2\alpha_{pq}(\mathbf{x}) \exp(\mathrm{i}\varepsilon_{1p} n_1 + \mathrm{i}\varepsilon_{2q} n_2), \tag{13}$$

where $\alpha_{pq}(\mathbf{x}) \equiv \alpha(\mathbf{x}, \varepsilon_{1p}, \varepsilon_{2q})$. These modes will satisfy the unit generalised mass condition, equation (12), provided that the wave amplitude functions $\alpha_{pq}(\mathbf{x})$ are scaled such that

$$(2N_1 N_2) \int_A \rho(\mathbf{x}) |\alpha_{pq}(\mathbf{x})|^2 \, \mathrm{d}\mathbf{x} = 1. \tag{14}$$

The use of equations (13) and (14) in equation (11) then leads to the result

$$w(\mathbf{n}, \mathbf{x}) = \sum_{p=1-N_1/2}^{N_1/2} \sum_{q=1-N_2/2}^{N_2/2} \frac{2F\alpha_{pq}^*(\mathbf{x}_0)\alpha_{pq}(\mathbf{x}) \exp[\mathrm{i}\varepsilon_{1p}(n_1 - n_{01}) + \mathrm{i}\varepsilon_{2q}(n_2 - n_{02})]}{[(1 + \mathrm{i}\eta)\Omega^2(\varepsilon_{1p}, \varepsilon_{2q}) - \omega^2]}, \tag{15}$$

where it has been assumed (without loss of generality for a highly damped system) that N_1 and N_2 are even, and the notation $\mathbf{n}_0 = (n_{01}, n_{02})$ has been employed. As explained in detail in reference [8], equation (15) strictly represents the contribution to the response arising from the modes which are associated with a *single* phase constant surface $\Omega(\varepsilon_1, \varepsilon_2)$. As remarked in section 2.2, multiple phase constant surfaces will normally arise, and in this case equation (15) must be summed over all the relevant surfaces. It is readily shown that each surface contributes a total of $N_1 N_2$ modes to equation (10), which is consistent with known results regarding the modal density of a two-dimensional periodic structure [18].

In reference [8] the summations which appear in equation (15) were converted into integrals over the ε_1–ε_2 plane, and the far field response of the system was evaluated by employing the method of stationary phase. With this approach care is needed to take due account of the presence of caustics, and the resulting analysis requires evaluation of the third derivatives of the phase constant surface $\Omega(\varepsilon_1, \varepsilon_2)$. In the present work the phase constant surfaces of the grillage system are computed numerically at discrete values of ε_1 and ε_2 by employing equation (9), and the numerical evaluation of the derivatives of a surface is prone to error unless a very fine grid of $(\varepsilon_1, \varepsilon_2)$ points is employed. For this reason it has been found to be more efficient for the present system to employ equation (15) directly rather than follow the more analytical approach described in reference [8].

Equation (15) enables the forced response of the grillage system to be computed if the phase constant surfaces $\Omega(\varepsilon_1, \varepsilon_2)$ and the associated wave amplitude functions $\alpha(\mathbf{x}, \varepsilon_1, \varepsilon_2)$ are known. As described in section 2, these quantities can readily be found by employing the hierarchical finite element method in conjunction with standard periodic structure theory. Results yielded by this approach are presented in section 5 for an example grillage system; as explained in the following section, the system considered has also been manufactured and tested experimentally.

4. DESCRIPTION OF THE TEST STRUCTURE

The periodic grillage test structure was constructed from an orthogonal array of aluminium strips as shown in Figure 3. The strips were of rectangular cross-section with an aspect ratio of approximately 12 : 1 (19·06 mm × 1·59 mm), and 14 strips were employed in the vertical direction while 13 strips were employed in the horizontal direction.

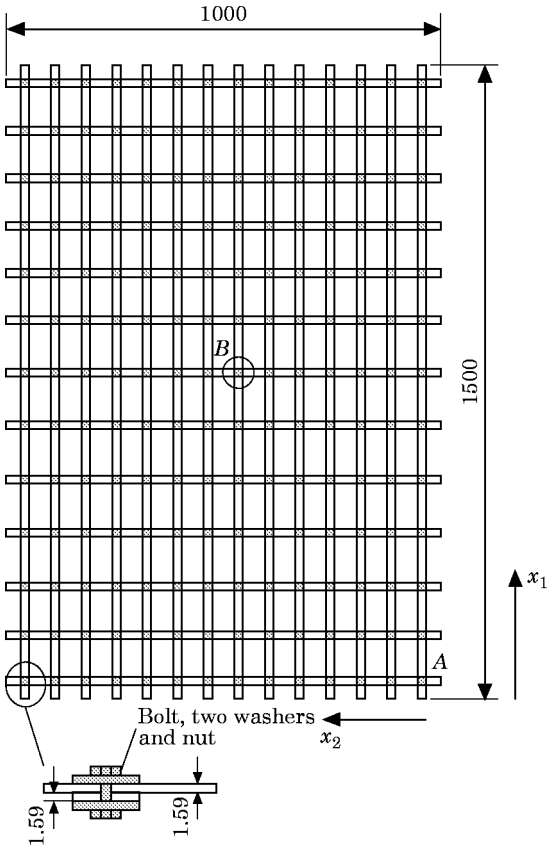

Figure 3. A schematic of the experimental structure. Note that the vertical direction is aligned with the x_1-axis shown in Figure 1, and the reference bolt position (A), $n_1 = n_2 = 1$, is located in the lower right-hand corner; the drive position is labelled B. All dimensions are in mm.

The vertical strips were more closely spaced than the horizontal strips, presenting a grillage aspect ratio of approximately 0·62 : 1 (the precise bolt spacings were 71·43 mm and 115·38 mm). At the crossing points, holes were drilled through both strips to accommodate the fasteners necessary to hold the assembly together: the mass of each set of washers, nut and bolt was approximately 6×10^{-3} kg and the total mass of the grillage (including bolt sets), was approximately 3·873 kg. One side of each strip was treated with a self-adhesive damping sheet supplied by Sound Service (Oxford) Ltd, reference SD1 SA. The mass of the complete structure, including the damping treatment, was 4·859 kg. The system was suspended on two thin steel cables from a supporting frame, and two small, soft pieces of foam were inserted between the frame and the grillage to prevent rigid body motion. The orientation of the experimental set-up (Figure 3) is such that the vertical direction coincides with the x_1-axis shown in Figure 1.

The structure was excited by means of an electromagnetic non-contacting shaker. The coil of the shaker was attached to a force transducer by using cyanoacrylate glue, and the force transducer was screwed directly to the bolt set of the grillage node (7, 7). An accelerometer was also mounted at this point; the effective mass of the transducer and accelerometer was found to be 4 g, and the raw signal from the force transducer was processed appropriately to produce the force actually applied to the grillage. The excitation consisted of white noise band-limited to 1550 Hz by means of a low-pass filter, and the

response at each grillage node was measured by means of a roving accelerometer and recorded at a sampling rate of 5350 Hz for 8192 samples. All data processing was performed by using the MATLAB basic toolbox [19], and all spectra and transfer functions were averaged over 20 realizations; the response of the system to harmonic forcing at any specified frequency in the range 0–1550 Hz could then be identified from the values of the transfer functions at this frequency.

The purpose of the damping treatment was to produce a non-reverberant structure, since the basic assumption which lies behind equation (15) is that the forced response is independent of the boundary conditions—this requires a sufficiently high level of damping to prevent the majority of the input disturbance from reaching the system boundaries. The system loss factor was found by dividing the measuring frequency range (from 0 to 1500 Hz) into 300 Hz frequency bands. For each band a Hanning window was implemented, and the impulse response function within each band was obtained by employing the inverse Fast Fourier Transform to the filtered signal. The damping was then estimated from the decay rate of the impulse response function [20, 21]. Without the damping treatment, the system was found to be highly reverberant, with a loss factor in the region of 0·005. With the damping treatment present the measured loss factor varied between 0·025 and 0·134 depending upon the measurement point (accelerometer location) and frequency band, with an average in the region of 0·1. For this reason a loss factor of 0·1 was adopted for the theoretical response predictions which are presented in the following section. Complete details of the experimental procedure are given in reference [22].

5. RESULTS

5.1. THEORETICAL RESULTS FOR THE PHASE CONSTANT SURFACES

As discussed in section 2.2, equation (9) governs free plane wave motion through the grillage: for specified values of the phase constants $-\pi < \varepsilon_i \leqslant \pi$ the equation yields multiple eigenfrequencies ω at which propagating wave motion can occur. These frequencies are normally presented graphically as surfaces over the ε_1–ε_2 plane, and computed results for the grillage described in the previous section are shown in Figures 4(a–d) in units of cycles per second $f\,(=\omega/2\pi)$. As detailed in section 2.1, a two-element model of a single period has been used to obtain these results, and in this case ten trial functions were employed in both equations (1) and (2). This leads to matrices **A** and **B** in equation (9) which are of dimension 34×34, and thus in principle 34 phase constant surfaces are yielded by the equation; only the first four surfaces, which are those shown in Figure 4, lie within the frequency range of interest.

It should be noted that some care is needed in the interpretation of the surfaces that are shown in Figure 4. The plots are arranged so that the lowest root ω (or f) yielded by equation (9) is shown in Figure 4(a), the second root is shown in Figure 4(b), and so on. This does not mean, however, that each plot represents a continuous function $\Omega(\varepsilon_1, \varepsilon_2)$; rather, the composite plot of Figures 4(a–d) represents a set of continuous surfaces $\Omega(\varepsilon_1, \varepsilon_2)$ which in some cases *intersect* each other. Thus Figure 4(a) represents a single continuous phase constant surface, whereas Figures 4(b) and 4(c) taken *together* represent two continuous phase constant surfaces which intersect. This feature is illustrated in Figure 5, which contains an outline plot of all four surfaces; the curve highlighted on the plane $\varepsilon_2 = -\pi$ is associated with a single continuous surface, and it can readily be seen that this surface is actually split between Figures 4(b) and 4(c).

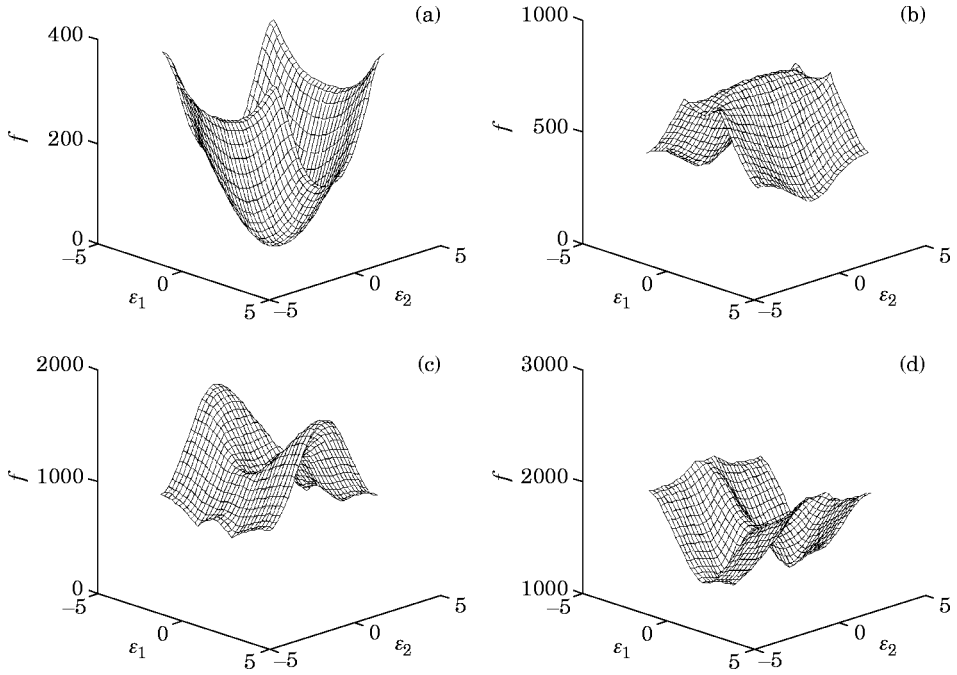

Figure 4. Phase constant surfaces for the beam grillage system: (a) first eigenfrequency; (b) second eigenfrequency; (c) third eigenfrequency; (d) fourth eigenfrequency.

The present work is concerned with harmonic excitation of the grillage at a specified frequency ω (or f)— a section through the phase constant surfaces at a fixed frequency will yield a contour on the ε_1–ε_2 plane, and a number of contours of this type are shown in Figure 6. As discussed in reference [8], the geometry of the contour associated with a particular value of f has a major influence on the nature of the response of the system to point harmonic forcing. Considering, for example, the $f = 600$ Hz contour shown in Figure 6(a), a point load will excite predominantly those propagating waves $(\varepsilon_1, \varepsilon_2)$ that lie on the contour; the energy flow associated with each wave lies along the local normal to the contour [18], and hence it is clear that the majority of the energy flow generated

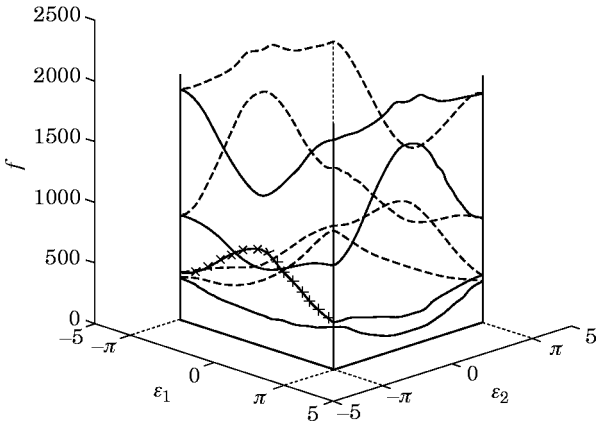

Figure 5. A composite outline plot of the first four phase constant surfaces. The second continuous surface is outlined on the $\varepsilon_2 = -\pi$ plane; it is clear that this surface contributes to both Figures 4(b) and 4(c).

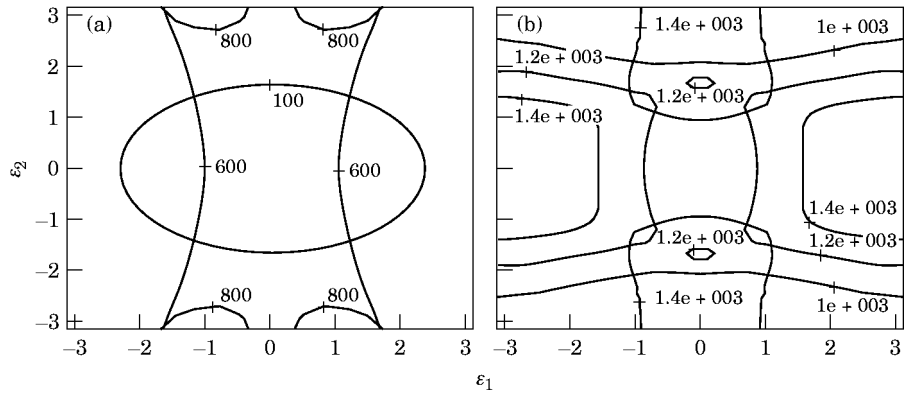

Figure 6. Fixed frequency contours of the phase constant surfaces: (a) 100 Hz, 600 Hz and 800 Hz; (b) 1 kHz, 1·2 kHz and 1·4 kHz.

by the point load will be in the x_1 direction. The response can therefore be expected to be confined to a fairly narrow "beam" which is aligned to the x_1-axis. In contrast, the $f = 100$ Hz contour is much more circular, and hence the forced response at this frequency can be expected to have a more uniform spatial distribution. Features of this type are clearly discernable in the forced response results which are presented in the following section.

5.2. THEORETICAL AND EXPERIMENTAL RESULTS FOR THE FORCED RESPONSE

Results for the forced response of the system are presented here in terms of contours of the normalized response $|w(n_1, n_2)/w(7, 7)|^2$, where $w(n_1, n_2)$ is the response at bolt position (n_1, n_2), and $w(7, 7)$ is the response at the drive point. The theory presented in section 3 is applicable to non-reverberant systems, and it has been found that the present system meets this requirement above 500 Hz; for this reason results are presented here for the forced response at 200 Hz intervals between 600 Hz and 1400 Hz. These results are shown in Figures 7–11 for (a) the experimental response contours and (b) the theoretical response contours, where the contours have been generated by using the contour facility of MATLAB [19], given the normalized response at each bolt point. By definition, the normalized response at the drive point is unity, and hence it is clear from Figures 7–11 that in each case the response falls off rapidly with increasing distance from this point, so that the system has the required property of being non-reverberant. Results have also

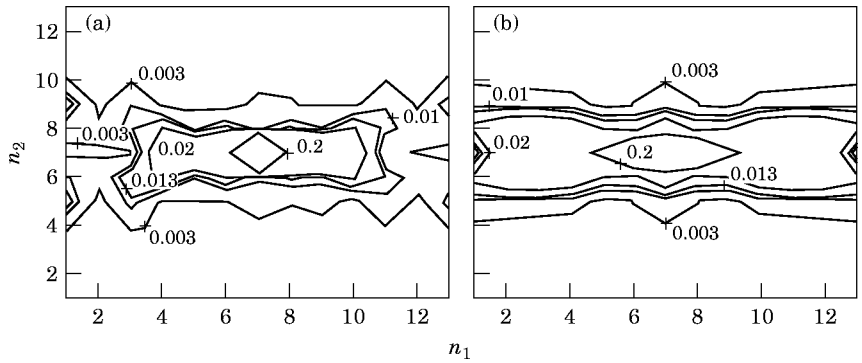

Figure 7. Normalized forced response contours $|w(n_1, n_2)/w(7, 7)|^2$ for $f = 600$ Hz. (a) experimental results; (b) theoretical results.

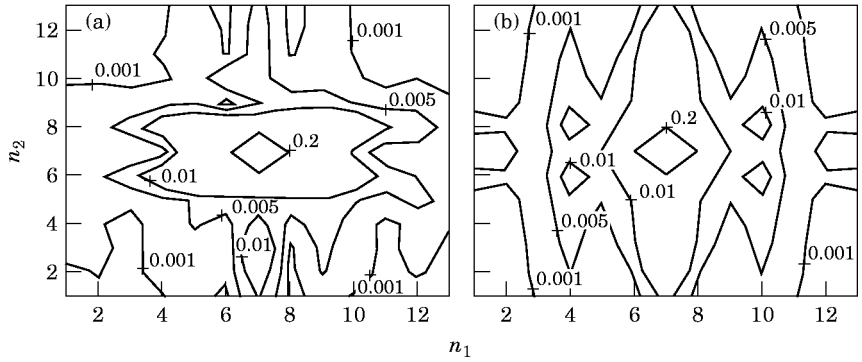

Figure 8. Normalized forced response contours $|w(n_1, n_2)/w(7, 7)|^2$ for $f = 800$ Hz. (a) experimental results; (b) theoretical results.

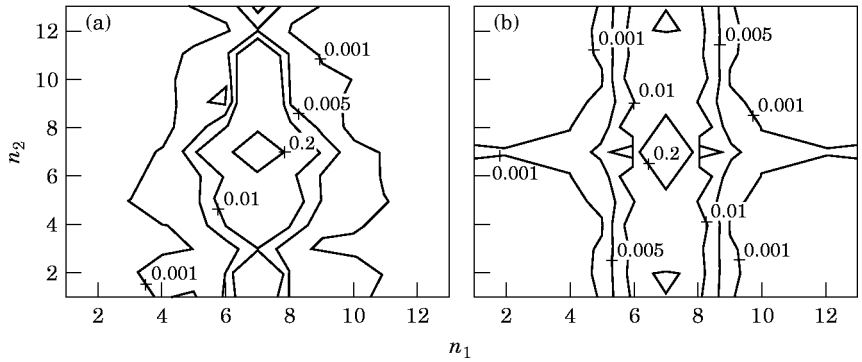

Figure 9. Normalized forced response contours $|w(n_1, n_2)/w(7, 7)|^2$ for $f = 1$ kHz. (a) experimental results; (b) theoretical results.

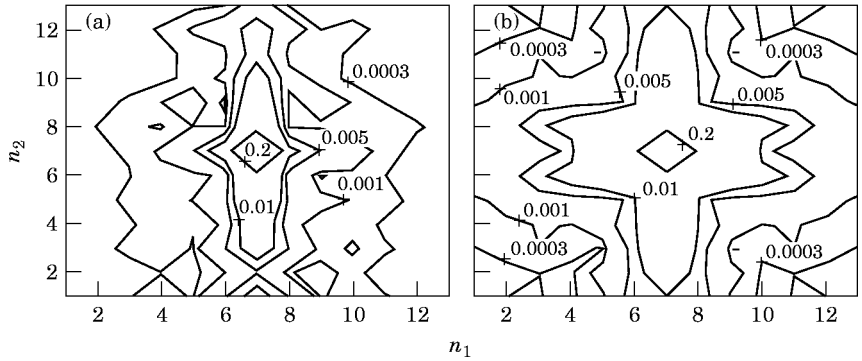

Figure 10. Normalized forced response contours $|w(n_1, n_2)/w(7, 7)|^2$ for $f = 1{\cdot}2$ kHz. (a) experimental results; (b) theoretical results.

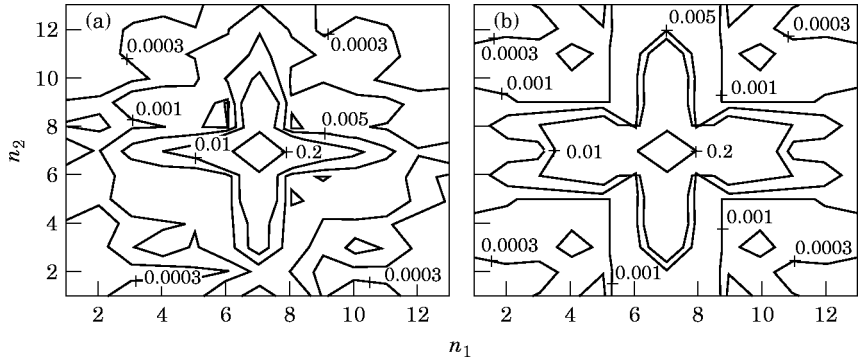

Figure 11. Normalized forced response contours $|w(n_1, n_2)/w(7, 7)|^2$ for $f = 1{\cdot}4$ kHz. (a) experimental results; (b) theoretical results.

been obtained for the response at many other frequencies between 600 Hz and 1400 Hz—these results confirm that there is a well defined progression between the results shown in Figures 7–11, so that all of the important physical features of the response are captured by the limited range of results presented here.

The physical implications of the geometry of the phase constant surfaces were considered in the previous section, and on this basis it was predicted that the energy flow generated by a point load at $f = 600$ Hz should be aligned predominantly to the x_1 direction. This prediction is borne out by both the experimental and theoretical results which are shown in Figure 7, where strong beaming in the x_1 direction is evident. The level of qualitative agreement between the theoretical and experimental results shown in Figure 7 is clearly very good, while the level of quantitative agreement is generally fair. In contrast, the level of agreement between theory and experiment shown in Figure 8 for the higher frequency $f = 800$ Hz is poor. The theoretical results show beaming in the x_2 direction, which is consistent with geometry of the $f = 800$ Hz contour shown in Figure 6: the normals to the contour are predominantly in the x_2 direction, which implies that the energy flow is also in this direction. This behaviour is not demonstrated by the experimental results at $f = 800$ Hz, although beaming of this type *is* obtained experimentally at 1 kHz, as shown in Figure 9. Considering Figures 7–9 together, it is clear that there is a transition from horizontal beaming to vertical beaming between 800 Hz and 1 kHz; both theory and experiment show this behaviour, although the theoretical transition frequency is somewhere below 800 Hz while the experimental transition occurs above this frequency.

The theoretical results at $f = 1{\cdot}2$ kHz shown in Figure 10 display beaming in both the x_1 and x_2 directions (with a low response along the lines $\pm 45^\circ$); again, this is consistent with the geometry of the $f = 1{\cdot}2$ kHz contour shown in Figure 6, in the sense that the normals to the contour are predominantly in the x_1 and x_2 directions. The experimental results shown in Figure 10 show beaming mainly in the x_2 direction, although beaming in both directions is clearly shown in Figure 11 for the higher frequency $f = 1{\cdot}4$ kHz. Both the experimental and theoretical results shown in Figures 9–11 display a transition from beaming in the x_1 direction to beaming in both the x_1 and x_2 directions, although, as for the previous transition between 600 Hz and 1 kHz, the precise transition frequency differs between theory and experiment.

Taken together, the results shown in Figures 7–11 show a broad measure of agreement between theory and experiment, particularly with regard to the occurrence of beaming and the phenomenon of transition between different types of beaming. At some frequencies the level of quantitative agreement between theory and experiment is relatively poor, and this can be traced in part to errors in the theoretical prediction of the transition frequencies. Possible sources of error lie in the modelling of the added damping treatment (which increased the mass of the system from 3·873 kg to 4·859 kg), the modelling of the bolted joints, and a lack of perfect periodicity in the experimental structure. The viscoelastic properties of the damping treatment were not readily available, and thus only a partial model of the mechanical behaviour of the material was included in the theoretical predictions. With regard to the bolted joints, only translational inertia was included in the model and with hindsight it is possible that rotational inertia could have played a non-trivial role for the test structure. Finally, it is known that structural imperfections can strongly influence the behaviour of a nominally periodic system [2], and the lightweight grillage system was noted to be slightly curved in the experimental configuration. Despite these reservations, it is thought that the level of agreement between theory and experiment is sufficient to validate the analytical predictions of reference [8] for a realistic engineering system.

6. CONCLUSIONS

In the Introduction it was stated that two points remained to be proven regarding the analysis contained in reference [8]: (i) whether "beaming" will occur for realistic two-dimensional periodic engineering structures; and (ii) whether beaming can be clearly observed in an experimental structure. With regard to point (i), the present theoretical study of a periodic beam grillage has shown that beaming can certainly occur in structures of this type; although not reported in any detail here, similar results have also been obtained by the authors for an orthogonally stiffened plate [22]. With regard to point (ii), beaming is clearly observable in the response of the present experimental beam grillage structure, and a reasonable level of agreement between theory and experiment has been obtained.

It should be emphasized that the present work has considered a non-reverberant system in which little of the power input at the drive point reaches the system boundaries. Under this condition the finite system behaves very like an infinite system, and the response is not affected by the nature of the boundary conditions. For a reverberant system the "beaming" behaviour observed here will constitute the direct field input from the drive point; the total response will include reflections from the system boundaries which may or may not obscure the beaming behaviour, depending on the boundary conditions. Many two-dimensional periodic engineering structures, such as orthogonally stiffened plates and shells, are actually relatively heavily damped due to the attachment of trim and acoustic treatment, as in the case of an aircraft fuselage structure. The present analysis has direct application to structures of this type, and it is conceivable that the beaming phenomenon could be exploited as a passive vibration isolation mechanism.

ACKNOWLEDGMENTS

The authors would like to thank the Brazilian Navy and the Directorate of Naval Engineering for the financial support of H. M. Ruivo during the course of this study. Thanks are also due to Professor F. J. Fahy of the University of Southampton for his help in administrative matters, and also for early discussions regarding the experimental structure.

REFERENCES

1. D. J. Mead 1996 *Journal of Sound and Vibration* **190**, 495–524. Wave propagation in continuous periodic structures: research contributions from Southampton 1964–1995.
2. S. S. Mester and H. Benaroya 1995 *Shock and Vibration* **2**, 69–95. Periodic and near-periodic structures.
3. L. Brillouin 1946 *Wave Propagation in Periodic Structures*. New York: Dover.
4. D. J. Mead, D. C. Zhu and N. S. Bardell 1988 *Journal of Sound and Vibration* **127**, 19–48. Free vibration of an orthogonally stiffened flat plate.
5. N. S. Bardell and D. J. Mead 1989 *Journal of Sound and Vibration* **134**, 55–72. Free vibration of an orthogonally stiffened cylindrical shell, II: discrete general stiffeners.
6. D. J. Mead 1990 *Journal of the Acoustical Society of America* **88**, 391–401. Plates with regular stiffening in acoustic media: vibration and radiation.
7. B. R. Mace 1980 *Journal of Sound and Vibration* **73**, 473–486. Periodically stiffened fluid-loaded plates, I: response to convected harmonic pressure and free wave propagation.
8. R. S. Langley 1996 *Journal of Sound and Vibration* **197**, 447–469. The response of two-dimensional periodic structures to point harmonic forcing.
9. R. S. Langley 1997 *Journal of Sound and Vibration* **201**, 235–253. The response of two-dimensional periodic structures to impulsive point loading.

10. D. M. Photiadis, E. G. Williams and B. H. Houston 1997 *Journal of the Acoustical Society of America* **101**, 877–886. Wave-number space response of a near periodically ribbed shell.
11. M. A. Heckl 1964 *Journal of the Acoustic Society of America* **36**, 1335–1343. Investigations on the vibrations of grillages and other simple beam structures.
12. R. D. Cook, D. S. Malkus and M. E. Plesha 1989 *Concepts and Applications of Finite Element Analysis*, *Third Edition*. New York: John Wiley.
13. N. S. Bardell, R. S. Langley, J. M. Dunsdon and T. Klein 1996 *Journal of Sound and Vibration* **197**, 427–445. The effect of period asymmetry on wave propagation in periodic beams.
14. N. S. Bardell 1989 *International Journal of Numerical Methods in Engineering* **28**, 1181–1204. The application of symbolic computing to the hierarchical finite element method.
15. L. Meirovitch 1986 *Elements of Vibration Analysis*. New York: McGraw-Hill.
16. R. S. Langley 1993 *Journal of Sound and Vibration* **167**, 377–381. A note on the force boundary conditions for two-dimensional periodic structures with corner freedoms.
17. J. M. Ziman 1965 *Principles of the Theory of Solid State Physics*. Cambridge: Cambridge University Press.
18. R. S. Langley 1994 *Journal of Sound and Vibration* **172**, 491–511. On the modal density and energy flow characteristics of periodic structures.
19. A. Biran and M. Breiner 1995 *MATLAB for Engineers*. Wokingham, Berkshire: Addison-Wesley.
20. F. Jacobsen 1987 *Journal of Sound and Vibration* **115**, 163–170. A note on acoustic decay measurements.
21. F. Jacobsen and D. Bao 1987 *Journal of Sound and Vibration* **115**, 521–537. Acoustic decay measurements with a dual channel frequency analyser.
22. H. M. Ruivo 1996 *M. Phil. Thesis*, *Department of Aeronautics and Astronautics*, *University of Southampton*. The forced response of two-dimensional periodic structures to harmonic point loading.